# Spontaneous Vesicle Formation and Phase Behavior in Mixtures of an Anionic Surfactant with Imidazoline Compounds

Yamaira I. González,[†] Maria Stjerndahl,[‡] Dganit Danino,[§] and Eric W. Kaler*,[†]

*Center for Molecular Engineering and Thermodynamics, Department of Chemical Engineering, University of Delaware, Newark, Delaware 19716, Department of Materials and Surface Chemistry, Chalmers University of Technology, Göteborg, Sweden, and Department of Biotechnology and Food Engineering, Technion Institute of Technology, Haifa, Israel 32000*

*Received March 12, 2004. In Final Form: May 11, 2004*

Unexpected colloidal assemblies form in aqueous mixtures of sodium dodecylbenzenesulfonate (SDBS) with the following imidazoline compounds: 2,2′-azobis[2-(2-imidazolin-2-yl)propane] dihydrochloride (V-44, which is a commonly used free-radical initiator), 2,2′-tetramethylenedi-2-imidazoline (TMI), and the main recombination product (RP) from the decomposition of V-44. All of these imidazoline compounds act as hydrotropes. As the molar ratio of imidazoline to SDBS increases, a gradual transition from micelles to vesicles to bilayers to precipitate is observed. V-44 decomposes slowly at 25 °C, and the phase diagrams of V-44/SDBS and RP/SDBS are similar. The vesicular region observed in mixtures of TMI/SDBS is larger in composition than that of V-44/SDBS and RP/SDBS mixtures. At equimolar compositions of SDBS and RP, a novel colloidal structure with multiple closely packed bilayers is observed. In these mixtures, small unilamellar vesicles (<80 nm in diameter) form spontaneously, although with time they coexist with a small amount of precipitate and their size increases steadily. The self-assembly of vesicles occurs over a wide range of compositions when the solution pH is lower than the p$K_a$ of the imidazoline moiety. Quasi-elastic light scattering, cryogenic transmission electron microscopy, nuclear magnetic resonance, and small-angle neutron scattering were used to determine the characteristic length scales and properties of the assemblies.

## Introduction

Unilamellar vesicles (ULV) can be the result of mixing cationic and anionic surfactants. This approach has attracted attention because the resulting structures form spontaneously and the surfactants used are inexpensive.[1−5] In addition, these vesicles have a final size dictated by surfactant composition and they are infinitely stable if solution conditions such as concentration, pH, and ionic strength are kept unchanged. Typically, the surfactants are single-tailed, but vesicles also form in mixtures containing double-chained surfactants, gemini surfactants, or mixtures of zwitterionic and ionic surfactants.[6]

Vesicles have also been observed in mixtures of single-tailed charged surfactants with oppositely charged hydrophobic ions. Examples are mixtures of cetyltrimethylammonium bromide (CTAB) with 5-methylsalicylic acid or with sodium 3-hydroxynaphthalene-2-carboxylate, aqueous solutions of alkyltrimethylammonium 5-ethylsalicylate surfactants ($C_n$TA5ES, with $n = 14$ or 16),[7] and mixtures of tetradecyldimethylamine oxide hemihydrochloride with sodium 2-naphthalenesulfonate.[8] Vesicles also form spontaneously in mixtures of the anionic double-tailed surfactant sodium bis(2-ethylhexyl) sulfosuccinate (AOT) with cholinergics and in solutions of the cationic double-tailed surfactant didodecyldimethylammonium hydroxide.[9] The hydroxide counterion and the choline chloride compounds control the curvature of the surfactant aggregate and thus set the type of microstructures formed.

Here, vesicles made of the common anionic surfactant sodium dodecylbenzenesulfonate (SDBS) and compounds containing imidazoline moieties at each end of the molecule are investigated. Special attention is given to 2,2′-azobis-[2-(2-imidazolin-2-yl)propane] dihydrochloride (V-44, Chart 1A), since V-44 is a water-soluble initiator often used in the polymerization of self-assembled surfactant aggregates[10] (e.g., micelles, vesicles, liquid crystals, and microemulsions) that are either made from polymerizable surfactants or are loaded with hydrophobic or hydrophilic monomers. Hubert et al. have shown that 2,2′-azobis(2-methylpropionamide)dihydrochloride (V-50), a similar water-soluble initiator,[11,12] transforms kinetically stabilized ULV of dioctadecyldimethylammonium ($DODA^+$)

* To whom correspondence should be addressed. Phone: 1(302) 831-3553. Fax: 1(302) 831-6751. E-mail: kaler@che.udel.edu.
[†] University of Delaware.
[‡] Chalmers University of Technology.
[§] Technion Institute of Technology.

(1) Kaler, E. W.; Murthy, A. K.; Rodriguez, B. E.; Zasadzinski, J. A. N. *Science* **1989**, *245*, 1371.
(2) Kaler, E. W.; Herrington, K. L.; Murthy, A. K.; Zasadzinski, J. A. N. *J. Phys. Chem.* **1992**, *96*, 6698.
(3) Herrington, K. L.; Kaler, E. W.; Miller, D. D.; Zasadzinski, J. A. N.; Chiruvolu, S. *J. Phys. Chem.* **1993**, *97*, 13792.
(4) Yatcilla, M. T.; Herrington, K. L.; Brasher, L. L.; Kaler, E. W.; Chiruvolu, S.; Zasadzinski, J. A. N. *J. Phys. Chem.* **1996**, *100*, 5874.
(5) Iampietro, D. J.; Kaler, E. W. *Langmuir* **1999**, *15*, 8590.
(6) (a) Marques, E. F.; Regev, O.; Khan, A.; da Graça, M. M.; Lindman, B. *J. Phys. Chem. B* **1998**, *102*, 6746. (b) Marques, E. F.; Regev, O.; Khan, A.; da Graça, M. M.; Lindman, B. *J. Phys. Chem. B* **1999**, *103*, 8353. (c) Caria, A.; Khan, A. *Langmuir* **1996**, *12*, 6282. (d) Bhattacharya, S.; De, S. *Langmuir* **1999**, *15*, 3400.
(7) (a) Lin, Z.; Cai, J. J.; Scriven, L. E.; Davis, H. T. *J. Phys. Chem.* **1994**, *98*, 5984. (b) Hassan, P. A.; Candau, S. J.; Kern, F.; Manohar, C. *Langmuir* **1998**, *14*, 6025. (c) Hassan, P. A.; Narayanan, J.; Menon, S. V. G.; Salkar, R. A.; Samant, S. D.; Manohar, C. *C. Colloids Surf., A* **1996**, *117*, 89. (d) Buwalda, R. T.; Stuart, M. C. A.; Engberts, J. B. F. N. *Langmuir* **2000**, *16*, 6780.
(8) Kawasaki, H.; Imahayashi, R.; Tanaka, S.; Almgren, M.; Karlsson, G.; Maeda, H. *J. Phys. Chem. B* **2003**, *107*, 8661.
(9) (a) Murthy, A. K.; Kaler, E. W.; Zasadzinski, J. A. N. *J. Colloid Interface Sci.* **1991**, *145*, 598. (b) Brady, J. E.; Evans, D. F.; Kachar, B.; Ninham, B. W. *J. Am. Chem. Soc.* **1984**, *106*, 4279.
(10) (a) Kline, S. R. *Langmuir* **1999**, *15*, 2726. (b) de Vries, R.; Co, C. C.; Kaler, E. W. *Macromolecules* **2001**, *34*, 3233. (c) Hentze, H. P.; Kaler, E. W. *Chem. Mater.* **2003**, *15*, 708.
(11) Liu, S.; González, Y. I.; Kaler, E. W. *Langmuir* **2003**, *19*, 10732.

10.1021/la0493464 CCC: $27.50 
Published on Web 07/21/2004

**Chart 1. Structure of (A) 2,2′-Azobis[2-(2-imidazolin-2-yl)propane] Dihydrochloride (V-44); (B) the Recombination Product (RP) of V-44, 2,3-Bis(imidazolin-2-yl)-2,3-dimethylbutane Dihydrochloride; and (C) 2,2′-Tetramethylenedi-2-imidazoline (TMI), Which Does Not Include the HCl Salt Present in V-44 and RP**

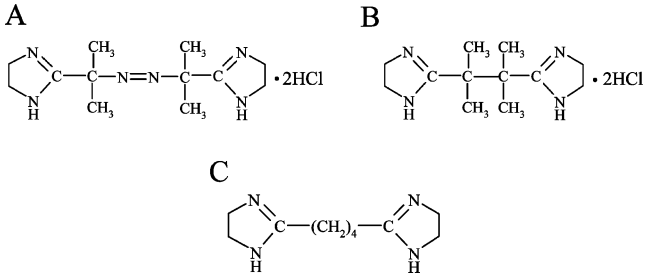


salts into twinned vesicles and unilamellar lens-shaped vesicles.[13] Likewise, the addition of V-50 to styrene-swollen DODABr ULV disrupts the vesicle architecture and changes the morphology of the polystyrene formed in the bilayer of these vesicles. V-44 has a molecular structure analogous to that of V-50, so it could also perturb the microstructure of SDBS micellar aggregates.

Since V-44 decomposes in water (it has a 6 day half-life at 25 °C), the phase behavior of mixtures of SDBS with two stable analogue species of V-44, 2,3(2-imidazolin-2-yl)-2,3-dimethylbutane dihydrochloride (the recombination product (RP), Chart 1B) and 2,2′-tetramethylenedi-2-imidazoline (TMI, Chart 1C), is also investigated. RP is structurally similar to V-44, but it lacks the cleavable azo group that yields radicals. Consequently, the (stable) RP molecule is shorter in length and stiffer than a V-44 molecule. On the other hand, TMI has a saturated chain of four carbon atoms, as opposed to the branched chain of RP, which results in a less rigid molecule whose length is closer to that of V-44.

This paper is organized as follows. First, the phase diagram and spontaneous microstructure formation in V-44/SDBS mixtures are described, with emphasis on characterization of the vesicle phase. The microstructures are determined using quasi-elastic light scattering (QLS), cryogenic transmission electron microscopy (cryo-TEM), nuclear magnetic resonance (NMR), and small-angle neutron scattering (SANS). Then, the phase diagram and microstructures in mixtures of RP/SDBS are reported and compared with the V-44/SDBS results. Finally, the spontaneous vesicle formation in mixtures of TMI/SDBS is also characterized and the transition from vesicle to precipitate is compared to that observed in mixtures of RP/SDBS and V-44/SDBS.

## Experimental Section

**Materials and Methods.** Hard-type (branched-chain)[14] SDBS was obtained from TCI America. V-44 and RP were supplied by Wako Chemicals (Richmond, VA), and $^{13}C$ NMR verified the RP structure. Sulfur, ethylenediamine, benzonitrile, and 1,4-dicyanobutane were purchased from Sigma-Aldrich. All chemicals were used as received.

TMI was synthesized from ethylenediamine and 1,4-dicyanobutane in the presence of sulfur according to the procedure described by Fischer et al.[15] The solid product was purified by washing in hot benzonitrile followed by recrystallization from a mixture of ethanol and acetone, giving a purity of more than 98% as confirmed by $^1H$ NMR.

Stock solutions of SDBS, V-44, RP, and TMI were prepared in deionized water (Milli-Q) or $D_2O$ (Cambridge Isotopes) and mixed at room temperature at the desired ratio. All the solution mixtures were gently shaken until a uniform-colored one-phase solution was observed. The solutions were not subjected to any type of mechanical agitation. V-44/SDBS, RP/SDBS, and TMI/SDBS samples were examined visually to determine the number of phases. Phase boundaries were assigned after the visual appearance of the samples remained unchanged with time. The phase behavior of mixtures at 25 °C is depicted using a pseudoternary phase representation. The results represent observations of ∼100 samples.

Transparent solutions were identified as micellar, while the vesicle phase was identified by an isotropic blue color. QLS was used to measure the size of the aggregates in each of the phases. Cryo-TEM and SANS were used to further characterize the morphology. For light scattering measurements, solutions made in either $D_2O$ or $H_2O$ were filtered through 0.45 $\mu$m poly(tetrafluoroethylene) (PTFE) filters and flame sealed in 1 mL ampules. For NMR studies, an aliquot of the samples was placed in NMR tubes and sealed. All samples were then kept during the equilibration and characterization studies in a thermostated bath at 25 °C.

In the titrations, all compounds were initially in the basic form, which is denoted as B−B. Solutions of V-44 and RP were treated with sufficient NaOH to bring the pH to ∼12. This was done because the two compounds were available as the dihydrochlorides, B−B·2HCl, so addition of NaOH allowed the in situ preparation of the free-base forms, B−B. TMI was already present in the free-base form.

**Surface Tension.** Surface tension measurements were made at 25 °C using a thermostated K10T digital tensiometer (Krüss) with a Wilhelmy plate. Before each measurement, the glassware was acid washed and rinsed with a sample of the solution at the desired concentration.

**Quasi-Elastic Light Scattering (QLS).** QLS was performed at 25 °C and at a 90° scattering angle using a Brookhaven BI-200SM goniometer, a BI9000AT digital correlator, and a Lexel 300 mW argon ion laser operated at 488 nm. The measured autocorrelation function was analyzed using CONTIN[16] to quantify the distribution of aggregates. The method of cumulants was also used to obtain the average decay rate ($<\Gamma>$).[17] The $z$-averaged hydrodynamic diameter ($D_h$) is obtained from the first cumulant by combining Stokes' law with the measured translational diffusion coefficient ($D$), $<\Gamma> = q^2D$. The polydispersity index was determined from the second moment $\mu_2 = \int_0^\infty(\Gamma - <\Gamma>)^2G(\Gamma)\,d\Gamma$. It is given by the relative variance $\mu_2/<\Gamma>^2$ and hence is a measure of the width of the decay rate distribution ($G(\Gamma)$).

**Nuclear Magnetic Resonance (NMR).** $^1H$ and $^{13}C$ NMR spectra were acquired using a Bruker AC250 NMR spectrometer (resonance frequency of 250 MHz for $^1H$) and a Bruker AMX360 spectrometer (resonance frequency of 360 MHz for $^1H$ and 90 MHz for $^{13}C$) operated at 25 °C.

**Light Microscopy (LM).** Small drops (∼150 $\mu$L) were placed on glass slides (Clay Adams) and covered with a cover slide. The specimens were examined at 25 °C using an Olympus BH-2 light microscope operated in differential interference contrast mode (DIC, Nomarski optics). Images from the light microscope were recorded using an Optronics 750 LE-D digital camera and processed using the Adobe Photoshop 7 ME software.

**Cryogenic Transmission Electron Microscopy (Cryo-TEM).** Specimens for cryo-TEM were prepared in a controlled environment vitrification system (CEVS) at saturation and a controlled temperature of 25 °C. The vitrified specimens were

(12) McKelvey, C. A.; Kaler, E. W.; Zasadzinski, J. A.; Coldren, B.; Jung, H.-T. *Langmuir* **2000**, *16*, 8285.

(13) Hubert, D. H. W.; Jung, M.; Frederik, P. M.; Bomans, P. H. H.; Meuldijk, J.; German, A. L. *Langmuir* **2000**, *16*, 8973.

(14) The approximate distribution of benzenesulfonate isomers is 4.4% $C_{10}$, 14.9% $C_{11}$, 66.0% $C_{12}$, 10.3% $C_{13}$, 4.4% $C_{14}$. The isomers are 100% branched. The calculations were performed by summing the peak areas in the branched and linear regions of the $C_{10}$−$C_{14}$ chromatograms which were obtained by the high performance liquid chromatography and mass spectrometry method. Smith, C.; Lynch, M. L., Procter & Gamble Co., Cincinnatti, OH, 2003.

(15) Fischer, T.; Lefebvre, H.; Fradet, A. *Macromol. Symp.* **1997**, *118*, 79.

(16) Provencher, S. W. *Comput. Phys. Commun.* **1982**, *27*, 229.

(17) Koppel, D. E. *J. Chem. Phys.* **1972**, *57*, 4814.

examined in a Philips CM120 transmission electron microscope operated at 120 kV using an Oxford 3500 cryo-holder maintained at below −178 °C. Images were recorded on a Gatan 791 MultiScan charge-coupled device (CCD) camera at low dose conditions using the Digital Micrograph 3.1 software. The size of spherical vesicles was measured from the digitized images using Scion Image software (Scion Corporation).

**Small-Angle Neutron Scattering (SANS).** Neutron scattering experiments were performed on the NG7 30 m spectrometer at the National Institute of Standards and Technology (NIST) in Gaithersburg, MD. Neutrons of wavelength $\lambda = 6$ Å with a spread of 11% were incident on samples held in quartz "banjo" cells with 2 mm path lengths. Three different sample-to-detector distances of 13.7, 4, and 1 m were used to cover an overall scattering vector ($q$) range of 0.003−0.53 Å$^{-1}$. The data were corrected for detector efficiency, background scattering, empty cell scattering, and sample transmission and placed on an absolute scale using NIST protocols and calibration standards. For data analysis, the ideal model scattering curves were smeared to take into account the instrument resolution.[18] The quality of the fit is assessed from the reduced $\chi^2$ values.

**SANS Analysis.** The SANS scattering curves of samples containing vesicles were fit using a polydisperse core−shell model where the vesicles are assumed to have a polydisperse core with constant shell thickness ($t$) and any intervesicle interactions are neglected.[19] In this case, for a polydisperse system of unilamellar noninteracting vesicles, the scattered intensity as a function of the scattering vector is given by

$$I(q) = \frac{d\Sigma}{d\Omega(q)} = n\int_0^\infty G(r_c)P^2(qr_c)\, dr_c \qquad (1)$$

where $n$ is the number density of vesicles, $P(qr_c)$ is the form factor of a single particle (e.g., vesicles) consisting of a core and an outer shell, and $G(r_c)$ is the normalized probability of finding a particle with a core radius between $r_c$ and $r_c + dr_c$. $G(r_c)$ is modeled as a Schulz distribution, so

$$G(r_c) = \frac{r_c^{\,Z}}{\Gamma(Z+1)}\left(\frac{Z+1}{\bar{r}_c}\right)^{Z+1} \exp\left(\frac{-r_c}{\bar{r}_c}(Z+1)\right) \qquad (2)$$

where $\bar{r}_c$ is the mean core radius and $Z$ is related to the variance ($\sigma^2$) of the core radius by

$$\frac{1}{Z+1} = \frac{\sigma^2}{\bar{r}_c^{\,2}} \qquad (3)$$

The form factor is

$$P(x) = \frac{4\pi}{q^3}(\rho_b - \rho_c)\left\{J_1\left(x + \frac{t}{r_c}x\right) - J_1(x)\right\} \qquad (4)$$

where $x$ is the dimensionless variable $qr_c$, $J_1(x) = \sin(x) - x\cos(x)$, and $\rho_b$ and $\rho_c$ are the scattering length densities (SLDs) of the bilayer and the core (taken as the solvent), respectively.

The SLDs were calculated by adding the scattering amplitudes of each group or atom in a molecule and dividing the total by the corresponding molecular volume. The SLD of $D_2O$ is $6.3 \times 10^{-6}$ Å$^{-2}$, and the SLD of the bilayers was calculated assuming the bilayer is made of an equimolar composition of the oppositely charged components. This assumption has little influence on the results.

The spectra from samples containing micelles were fit to a model incorporating an ellipsoidal form factor. The Hayter and Penfold rescaled mean spherical approximation together with the Yukawa form of the potential between the micellar "macroions" was used to account for interparticle interactions in terms of the structure factor $S(q)$.[20] The intensity model for monodisperse, interacting ellipsoidal micelles is

$$I(q) = \frac{d\Sigma}{d\Omega(q)} = n\int_0^1 |F(q,\mu)|^2\, d\mu\left(1 + \frac{\langle F(q,\mu)\rangle^2}{\langle |F(q,\mu)|^2\rangle}(S(q) - 1)\right) \qquad (5)$$

with

$$F(q,\mu) = v(\rho_m - \rho_s)\frac{3j_1(u)}{u} \qquad (6)$$

and

$$u = q[a^2\mu^2 + b^2(1-\mu^2)]^{0.5} \qquad (7)$$

where $a$ is the semimajor axis of the micelle, $b$ is the semiminor axis, $v$ is the volume of the micelles, $\rho_m$ and $\rho_s$ are the coherent scattering length densities of the micelle and the solvent, respectively, and $j_1(u)$ is the first order spherical Bessel function.

For model calculations, the ionic strength was initially fixed by the sum of the concentrations of unassociated surfactant molecules at the critical aggregation concentration (∼0.4 mM); the concentration of imidazoline molecules, which is twice the concentration of V-44 or RP species, since both ends of the molecule are protonated; and with the assumption of 10% ionization of the micelles. The adjustable parameters were the semiminor radius ($b$), the semimajor axis ($a$), and the net charge of the surfactant−hydrotrope micelles. If $b > a$, the micelles are oblate ellipsoids, while, if $b < a$, the micelles are prolate ellipsoids. The fitted parameters minimized the value of $\chi^2$ for the model fit of each SANS spectrum.

## Results

**Properties of V-44 and the V-44 Analogues.** V-44 (Chart 1A) decomposes in aqueous solutions to form $N_2$ and two (2-imidazolin-2-yl)propyl radicals that can initiate a free-radical polymerization. In the absence of monomers, the radicals produce a variety of side products, as documented by the appearance of new signals in the $^1$H NMR and $^{13}$C NMR spectra. However, the main decomposition product is a stable analogue species that forms when two radicals recombine. This recombination product (RP) is shown in Chart 1B. At 25 °C, this decomposition has ∼75% selectivity toward RP as measured by NMR.

Titrations with HCl converted the free-base forms (B−B) of the imidazoline compounds first to the monoprotonated form ($^+$HB−B) and then to the diprotonated form ($^+$HB−BH$^+$). Two titration stages were not resolved, so the p$K_a$ values for both imidazoline groups are similar. The titration of both groups required 2 equiv of HCl. Therefore, the pH at the midpoint is approximately the p$K_a$ value of these functional groups. For both V-44 and RP, this p$K_a$ is between 9.7 and 10. Thus, at pH 6, which is the pH of a 50 mM stock solution due to the presence of HCl, both imidazoline groups are protonated. Likewise, the imidazoline end groups present in the synthesized material TMI (Chart 1C) have an average p$K_a$ of ∼11. Stock solutions of 50 mM TMI have a pH of 11, so at this pH value, ∼50% of the imidazoline end groups are protonated.

**Aggregation Behavior.** V-44 is a weakly surface-active compound in water. The surface tension of a solution of 835 mM V-44 is 40 mN/m (Figure 1). At 841 mM, the solution is saturated and two phases form. Addition of V-44 to solutions of SDBS favors the formation of mixed aggregates. At molar ratios of 1:3 and 1:1.25 V-44/SDBS, V-44 reduces by 10-fold the concentration at which colloidal aggregates form in SDBS solutions. V-44 also lowers the ultimate surface tension from 31 mN/m for SDBS in water to 26 mN/m for the mixture. Similar behavior is found for mixtures of RP/SDBS and TMI/SDBS (not shown).

(18) Barker, J. G.; Pedersen, J. S. *J. Appl. Crystallogr.* **1995**, *28*, 105.
(19) Bartlett, P.; Ottewill, R. H. *J. Chem. Phys.* **1992**, *96*, 3306.
(20) Hansen, J. P.; Hayter, J. B. *Mol. Phys.* **1982**, *46*, 651.

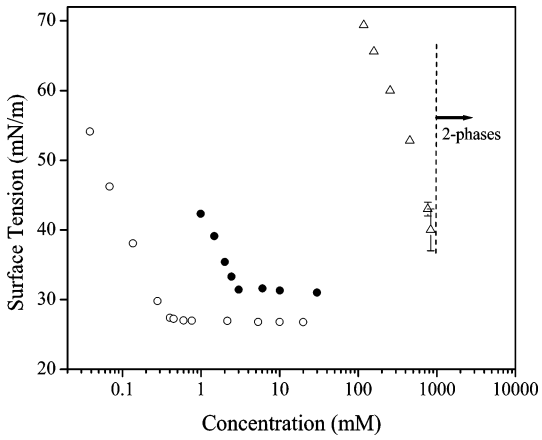


**Figure 1.** Surface tension at 25 °C of an aqueous solution of (△) V-44, (●) SDBS, and (○) a 1:3 molar ratio of V-44/SDBS. The V-44 solution does not exhibit the characteristic minimum in surface tension observed with other hydrotropes but rather reaches its solubility limit and phase separates. Larger uncertainties are observed for surface tension measurements closer to the solubility phase boundary. SDBS displays a cmc value of 3 mM, and the 1:3 mixture displays a critical aggregation concentration (cac) of 0.4 mM. In mixtures of SDBS with V-44, RP, or TMI, the surface tension is lowered to 26 mN/m at the cac.

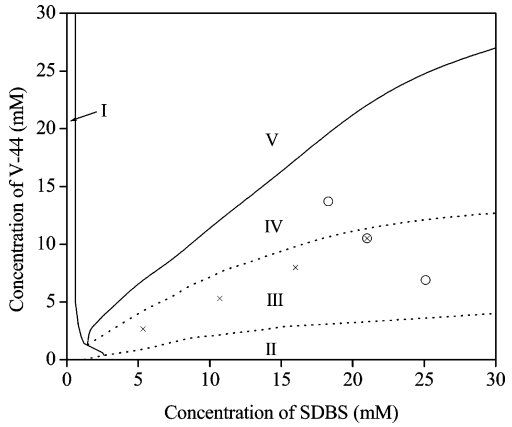


**Figure 2.** Water-rich corner of the pseudoternary phase diagram of V-44/SDBS/water at 25 °C after 6 months of aging. The phase regions are monomeric SDBS and products from the decomposition of V-44 (RP is the main component of decomposition) (I), micelles (II), vesicles (III), bilayers and vesicles coexisting with a large amount of precipitate (IV), and precipitate (V). The phase transitions from unilamellar vesicles to bilayers coexisting with precipitate and from vesicles to micelles occur gradually, therefore the dashed curve. The phase boundaries from bilayers to precipitate and from monomeric SDBS to precipitate are marked by sharp transitions. The × symbols represent samples along a dilution path that were aged and characterized with QLS and SANS. The ○ symbols mark sample compositions at different ratios of V-44/SDBS that were characterized with SANS.

**V-44/SDBS Mixtures. (a) Phase Behavior.** Figure 2 shows part of a pseudoternary phase diagram of the V-44/SDBS/$H_2O$ system at 25 °C after 6 months of equilibration (6 months corresponds to 30 V-44 half-lives). Along the binary axis of V-44−$H_2O$, solutions are transparent at all V-44 concentrations studied (region I in Figure 2). There is no evidence that the initiator or its decomposition products form any microstructure in water. With the addition of 1 mM SDBS and for molar ratios of V-44/SDBS > 1, precipitate is observed. Transparent solutions are also observed along the SDBS−$H_2O$ axis for mixtures containing a small amount of V-44 (region II). Throughout this regime, QLS measurements indicate the presence of aggregates smaller than 15 nm. Cryo-TEM (Figure 3B) confirms the presence of micelles of ∼4 nm in diameter coexisting with larger aggregates of ∼10−14 nm that form with aging of the sample. A duplicate sample aged for 2 weeks only shows spheroidal micelles (Figure 3A), and a CONTIN analysis yields a distribution of sizes smaller than 6 nm.

Upon further addition of V-44, bluish solutions are obtained after only gentle mixing of stock solutions of each material, suggesting spontaneous formation of vesicles, which have hydrodynamic diameters between 50 and 60 nm. The size and morphology of the structures evolved with time. After an aging period of 1 month, three different phase regions developed and persisted for over 6 months. Each is described below and highlighted in Figure 2.

At V-44/SDBS molar ratios greater than 1 (region V), a two-phase mixture of precipitate under a transparent supernatant is observed. Near the equimolar region (region IV), a turbid dispersion coexists with precipitate. More precipitate is observed as equimolar compositions are approached by moving vertically in the phase diagram at a fixed SDBS concentration with increasing amounts of V-44. In contrast, all samples in the vesicle region (region III) retain their isotropic blue color. In this region, a small turbid cloud or a "wisp" of precipitate similar to that described by Yatcilla et al.[4] is often observed coexisting with the vesicular solution. This cloud, which is present in very small quantities, forms within a few days of mixing the stock solutions and can be easily redispersed if the solutions are disturbed. Because the wisp settles out of the laser beam path, it does not affect the QLS measurements.

**(b) Vesicle Microstructures: QLS and SANS Results.** Four different V-44/SDBS compositions (in $D_2O$) at a constant molar ratio of 1:2 were aged, and the change in the vesicle size was measured by QLS over time (Figure 4). These samples follow the dilution path highlighted by the × symbols in Figure 2. After 6 months of equilibration, the vesicles reach hydrodynamic diameters of 75−115 nm. The size drop observed at 40 days for the most concentrated sample (32 mM total concentration of hydrotrope plus surfactant) is accompanied by precipitate formation. Once the precipitate has settled, the remaining vesicles continue to age and appear to reach a constant size. The aggregates in this sample have a polydispersity of 0.26, while the polydispersity for the most dilute samples remains constant at 0.14−0.16. Note also in Figure 4 that the vesicle size increases with decreasing surfactant concentration, as was also shown for catanionic vesicles of cetyltrimethylammonium tosylate (CTAT) and SDBS.[12]

Figure 5 shows neutron scattering spectra for three of these V-44/SDBS samples after aging for 45 days. Hydrodynamic diameters of 77, 86, and 88 nm were measured by QLS for the 32, 24, and 16 mM samples, respectively. At intermediate $q$ values, the curves are characterized by a $q^{-2}$ decay, which is a signature of scattering from a bilayer structure. All curves exhibit an inflection point in the range $0.008\ Å^{-1} < q < 0.015\ Å^{-1}$ that is related to the extent of polydispersity. With account of wavelength smearing, the SANS data are well described by a model of polydisperse core−shell vesicles of constant bilayer thickness (solid lines). The sharper minima for the model curves at $q > 0.15\ Å^{-1}$ are due to the lower signal-to-noise ratio. The fitted parameters yield a vesicle diameter, polydispersity, and bilayer thickness (Table 1), all of which are roughly the same for each sample. The fitted number average diameters of ∼58 nm are less than the $z$-averaged hydrodynamic diameter, as expected for a polydisperse population.

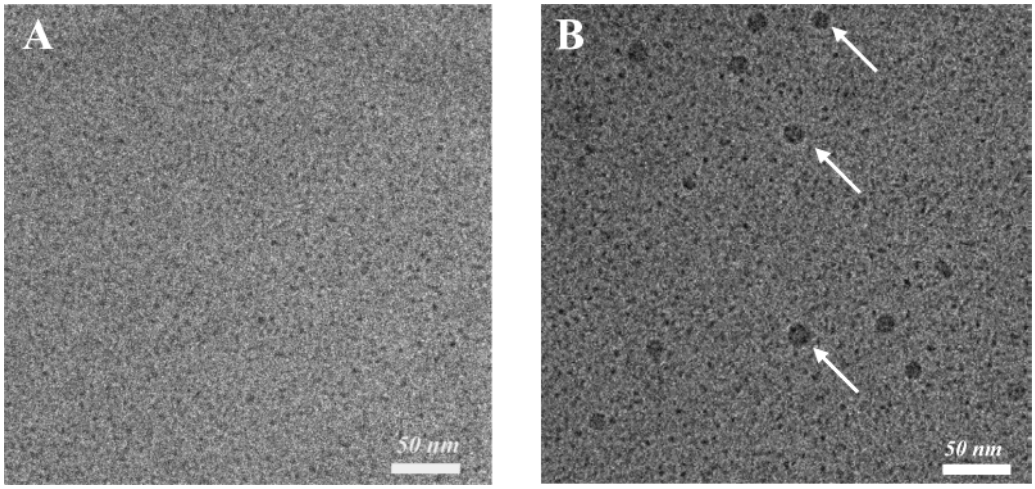


**Figure 3.** Cryo-TEM micrographs from a 2.5 mM V-44 and 20 mM SDBS sample that is located within the micellar region (region II) after aging for two different periods: (A) 2 weeks of aging—only 4 nm micelles are observed; (B) 6 months of aging—two populations exist in the mixture, namely, the 4 nm micelles (also present in the left panel) and the 10−14 nm spherical structures (white arrows), which are probably precipitate.

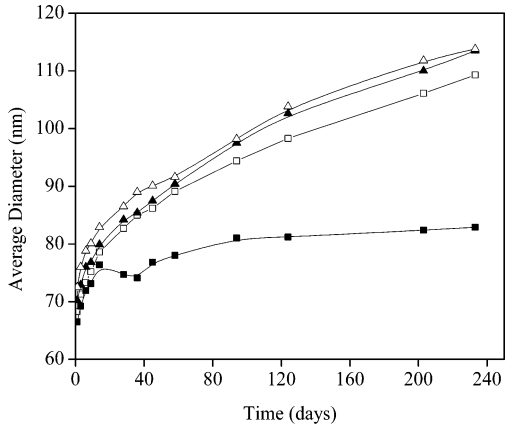


**Figure 4.** Size evolution (*z*-average diameter) of V-44/SDBS vesicles (region III) at 25 °C measured with QLS. The size of the aggregates continues to increase after 6 months. All solutions are from the dilution path indicated in Figure 2 with a V-44/SDBS mixing ratio of 1:2 and have a blue isotropic color: (△) 8 mM; (▲) 16 mM; (□) 24 mM; (■) 32 mM. A small quantity of an easily redispersable second phase in the form of a "wisp" or small cloud is observed in all samples. The wisp settles out of the laser beam path and does not influence the QLS measurements. If the wisp is redispersed and the QLS measurements are done immediately after, the measured size will be ∼2 nm higher.

**Table 1. Results from Fitting the Smeared Polydisperse Core−Shell Model to the SANS Spectra from Samples Containing Vesicles at Increasing Dilution and a Constant V-44/SDBS Molar Ratio of 1:2 (Figure 5)[a]**

| total concn (mM) | outer diameter (nm) | poly-dispersity | bilayer thickness (nm) | vesicle volume fraction (%) | $\sqrt{\chi^2/N}$ |
|---|---|---|---|---|---|
| 32 | 60 ± 1 | 0.28 ± 0.02 | 2.3 ± 0.1 | 4.0 | 2.6 |
| 24 | 59 ± 1 | 0.28 ± 0.01 | 2.3 ± 0.1 | 2.9 | 2.6 |
| 16 | 56 ± 1 | 0.30 ± 0.01 | 2.2 ± 0.1 | 1.9 | 2.0 |

[a] The quality of the fits is assessed from the reduced $\chi^2$ error between model and data.

Scattering data for samples prepared at different V-44/SDBS molar ratios and a constant total molar concentration of 32 mM (open circles, Figure 2) are plotted in Figure 6. The sample with a molar ratio of 1:1.3 V-44/SDBS is within the bilayer region and 1:2.0 V-44/SDBS is in the vesicular region, while 1:3.7 V-44/SDBS is closer to the micellar phase boundary. All the scattered intensities decay as $q^{-2}$, and all can be fit by a polydisperse core−shell model (Table 2).

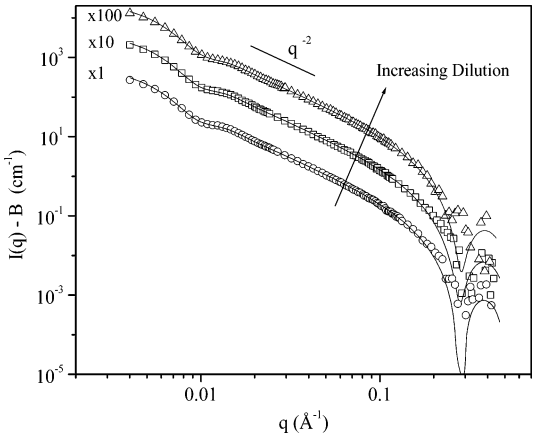


**Figure 5.** SANS spectra for samples within the vesicle region at increasing dilution and a constant V-44/SDBS molar ratio of 1:2. The total surfactant concentrations are (○) 32 mM, (□) 24 mM, and (△) 16 mM. The open symbols represent the experimental data and the solid lines the fit to the experimental data using a smeared polydisperse core−shell model. The spectrum at 32 mM is on an absolute scale, and subsequent spectra are shifted upward by factors of 10 and 100 for clarity.

**Table 2. Results from Fitting the Smeared Polydisperse Core−Shell Model to the SANS Spectra from V-44/SDBS Samples Containing Vesicles and with a Total Molar Concentration of 32 mM (Figure 6)[a]**

| V-44/SDBS molar ratio | outer diameter (nm) | poly-dispersity | bilayer thickness (nm) | vesicle volume fraction (%) | $\sqrt{\chi^2/N}$ |
|---|---|---|---|---|---|
| 1:1.3 | 58 ± 4 | 0.41 ± 0.06 | 3.1 ± 0.2 | 2.5 | 5.2 |
| 1:2.0 | 60 ± 1 | 0.28 ± 0.02 | 2.3 ± 0.1 | 4.0 | 2.6 |
| 1:3.7 | 66 ± 1 | 0.24 ± 0.01 | 1.7 ± 0.1 | 8.5 | 5.1 |

[a] The quality of the fits is assessed from the reduced $\chi^2$ error between model and data.

**(c) Vesicle Microstructures: Cryo-TEM and Light Microscopy Results.** Light and electron microscopy studies of samples of various compositions of V-44/SDBS show that the size, shape, and distribution of structures vary with the relative composition of the two components. Figures 7 and 8 show representative images.

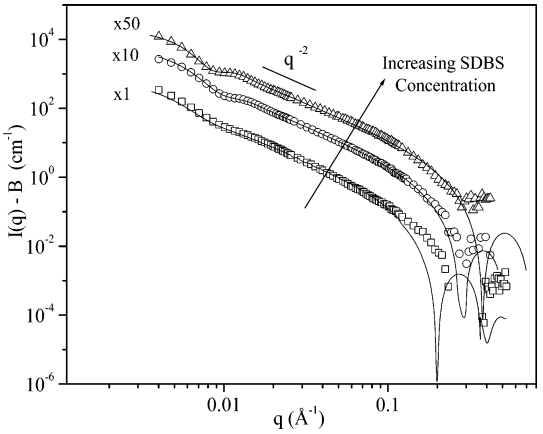


**Figure 6.** SANS spectra for samples at different ratios of V-44/SDBS and a total molar concentration of 32 mM. The molar ratios of V-44/SDBS are (□) 1:1.3, (○) 1:2.0, and (△) 1:3.7. The open symbols represent the experimental data and the solid lines the fit to the experimental data using a smeared polydisperse core−shell model. The spectrum at a molar ratio of 1:1.3 V-44/SDBS is on an absolute scale, and subsequent spectra are shifted upward by factors of 10 and 50 for clarity.

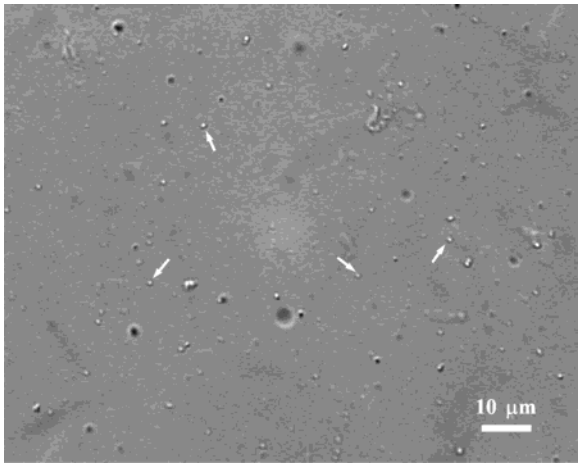


**Figure 7.** Light microscopy image showing vesicles of up to 1 $\mu$m in diameter that are present in a 10 mM V-44 and 2.5 mM SDBS mixture (region V). This image was recorded 1 week after mixing the stock solutions of V-44 and SDBS. At that time, the solution was turbid. Over time, the solution evolves into a two-phase mixture of precipitate and transparent supernatant.

Within region V, aggregates grow rapidly upon mixing stock solutions of V-44 and SDBS and eventually reach the final state of precipitate shown in the phase diagram. Vesicles of up to 1 $\mu$m in diameter are found by light microscopy in a sample of 10 mM V-44 and 2.5 mM SDBS (Figure 7) aged for 1 week. At equimolar compositions (along the V−IV boundary), the vesicle diameters observed by cryo-TEM ranged from 15 to 800 nm (Figure 8A and B). Smaller vesicles with a narrower size distribution were found in region IV (see, for example, Figure 8C), and even smaller and more uniform vesicles exist in region III, although a few large vesicles of up to 300 nm in diameter were seen at all the compositions studied within the vesicular phase.

Figure 8D shows a typical cryo-TEM image of a sample near the center of the vesicle lobe (5 mM V-44 and 15 mM SDBS, region III) after 1 month of equilibration. Mostly unilamellar vesicles ranging from 30 to 75 nm in diameter are found, although a small fraction of larger vesicles is also seen. The size distributions of the vesicle radius measured by cryo-TEM for ~2000 spherical vesicles after 1 month and after 6 months of aging are shown in Figure 9. The number average vesicle diameter is $<D_n> = 50$ nm and $\sigma/<D_n> = 0.43$ for the 1 month old sample, while for the 6 month old sample $<D_n> = 50$ nm and $\sigma/<D_n> = 0.50$. For this sample, a *z*-average diameter of 73 nm and a polydispersity of 0.10 were measured by QLS after 1 month of aging.

It is not surprising that QLS results of the average size of these vesicles are greater than those determined by cryo-TEM. It is well-known that the size measured by QLS is an intensity-average value that more heavily weights the larger structures in solution.[21] For the same reason, and as shown by Liu et al.[11] for catanionic vesicles made from polymerizable surfactants, QLS values should also be larger than size data obtained from SANS measurements. Both patterns are observed for the vesicle results presented here.

**(d) Phase Transition: NMR Studies.** NMR was used to follow the transitions from micelles to vesicles to precipitate. The signals were analyzed in terms of corresponding changes of the interface rigidity[22,23] of aggregates formed in V-44/SDBS mixtures. This is accomplished by studying 15 mM SDBS solutions with varying V-44 amounts 1 day after mixing the stock solutions. Figure 10A shows the NMR spectrum of a 5 mM solution of V-44. The signals at $\delta = 4.0$ and 1.5 ppm correspond to the methyl protons and the $-CH_2$ groups in the imidazoline ring, respectively. On the other hand, the spectrum of a 15 mM solution of SDBS (Figure 10B) shows two chemical shifts at $\delta = 7.7$ and 7.3 ppm that correspond to the ortho and meta protons of the aromatic group, respectively. The peaks below 2 ppm arise from the protons in the alkyl chain and are evidence that the surfactant is highly branched.

With addition of 2.5 mM V-44 to a 15 mM solution of SDBS (yielding a composition still in the micellar region), the resonance lines of SDBS broaden. A new signal at $\delta = 3.7$ ppm is also observed (Figure 10C), which can be attributed to the protons in the imidazoline groups. The line has shifted upfield 0.3 ppm from the usual chemical shift of pure V-44. The peak of the methyl protons of V-44 should appear slightly below $\delta = 1.5$ ppm, but it is obscured by the SDBS signal. The line broadening and upfield shift indicate the intercalation of V-44 end groups among the SDBS headgroups and suggest that there are strong interactions between the imidazolines and the surfactant headgroups.[22,23]

Upon addition of 5 mM V-44, vesicles form in $D_2O$. The corresponding NMR spectrum (Figure 10D) shows that the lines of the SDBS aromatic protons and the V-44 imidazoline protons disappear. Sharp signals from both lines of V-44 (Figure 10E) are observed again upon further addition of V-44. At higher V-44 concentrations, the V-44 lines increase in magnitude (Figure 10F) and shift further downfield toward the chemical shifts characteristic of V-44. The appearance of these lines and their shift indicate there is an excess of V-44 in solution. Over time, precipitate is observed in samples with excess V-44. This is reflected by the decrease in the intensity of the V-44 signals compared with the solvent line (not shown). Likewise, small peaks from the decomposition of V-44 appear in the spectra at later times.

(21) Coldren, B.; van Zanten, R.; Mackel, M. J.; Zasadzinski, J. A. *Langmuir* **2003**, *19*, 5632.
(22) Salkar, R. A.; Mukesh, D.; Samant, S. D.; Manohar, C. *Langmuir* **1998**, *14*, 3778.
(23) Soltero, J. F. A.; Puig, J. E.; Manero, O.; Schulz, P. C. *Langmuir* **1995**, *11*, 3337.

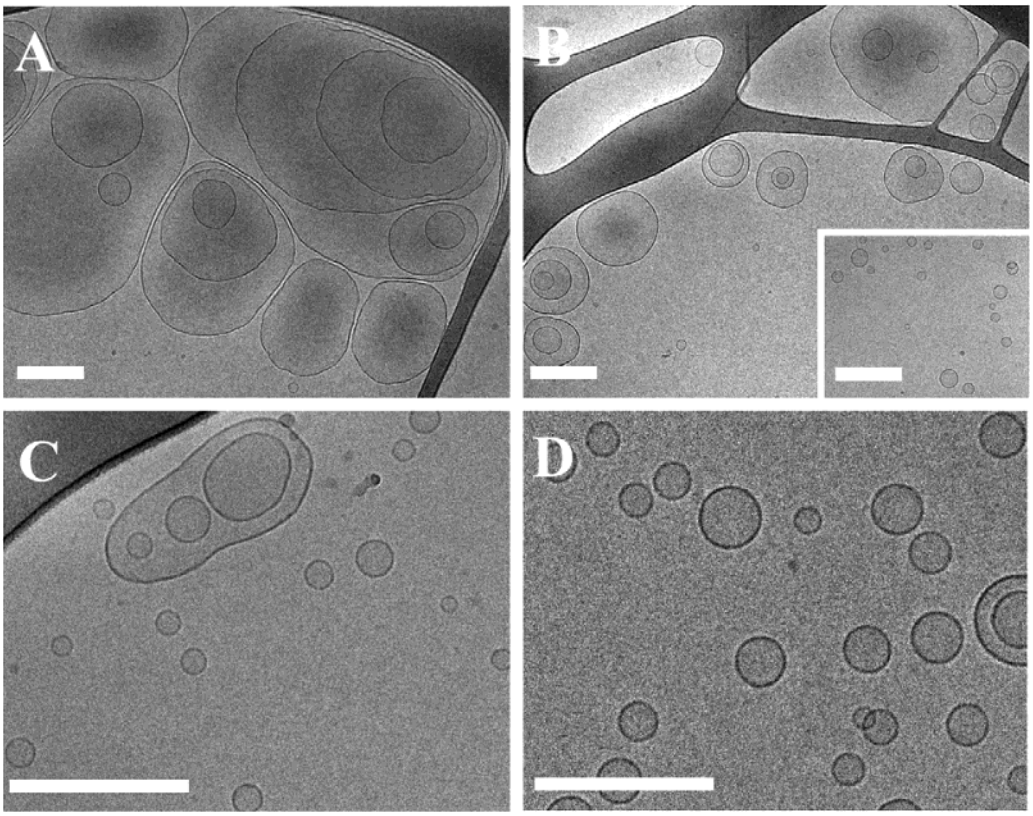


**Figure 8.** Smaller and more uniform vesicles form in V-44/SDBS and RP/SDBS mixtures as the composition changes from region V to region III. Along the equimolar composition (V−IV boundary), large and small vesicles coexist, as seen in parts A and B for the 20 mM V-44/SDBS mixture. Smaller vesicles form (part C) within region IV (15:20 mM V-44/SDBS), and rather small and uniform unilamellar vesicles are found in region III, as seen in part D for a 5 mM V-44 and 15 mM SDBS mixture after equilibration for 1 month. The micrographs in parts B and C are representative of the aggregate structures observed in mixtures of TMI·2HCl/SDBS. Bars = 200 nm.

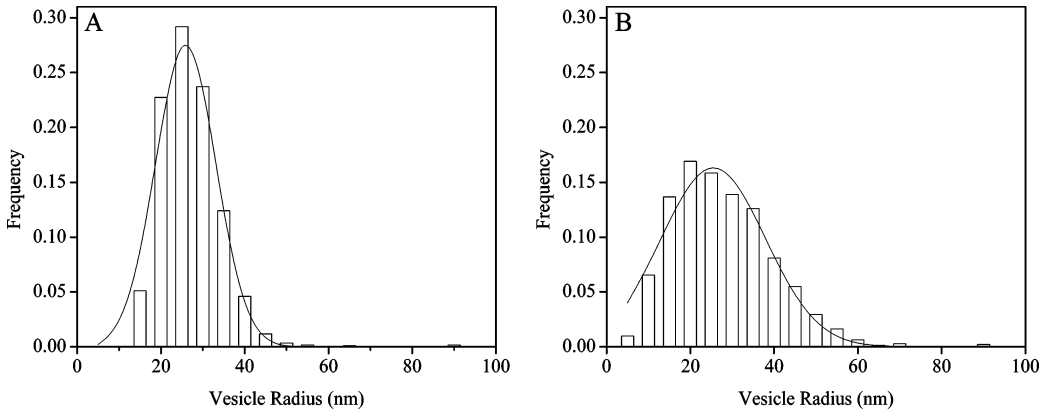


**Figure 9.** (A) Vesicle size distribution histogram of the V-44/SDBS vesicles shown in Figure 8D (after 1 month of aging) determined from measurements of ~2000 vesicles imaged by cryo-TEM. About 0.2% of the vesicles have a radius larger than 100 nm and were not plotted in the histogram. (B) Vesicle size distribution for the same sample after 6 months of aging. Unilamellar vesicles are also observed, but the size distribution has broadened. The number average diameters based on the raw numerical data from cryo-TEM are (A) 50 nm and (B) 51 nm, respectively. The solid curve in each plot is the best fit of the bending rigidity model derived by Jung et al.[27] for (A) $K = (0.35 \pm 0.02)k_BT$ and $R_0 = 30.0 \pm 0.4$ nm and for (B) $K = (0.16 \pm 0.01)k_BT$ and $R_0 = 46 \pm 3$ nm. These parameters indicate that the vesicles are stabilized by Helfrich fluctuations.

**Microstructures in RP/SDBS Mixtures.** The phase diagrams of RP/SDBS and V-44/SDBS mixtures are qualitatively similar. The visual appearance of RP/SDBS mixtures stabilizes after 2 weeks, while 1 month was required for the different phase regions to fully develop in V-44/SDBS mixtures.

**(a) Micelles: SANS Results.** Figure 11 shows scattering data (open squares) together with the model fit for a RP/SDBS sample in the micellar region. The presence of a peak at $q \sim 0.05$ Å$^{-1}$ indicates repulsive intermicellar interactions. The data are fit using the standard model of an ellipsoidal form factor together with the Hayter and Penfold rescaled mean spherical approximation for the structure factor. The data can be fit with either an oblate or a prolate ellipsoid model. The oblate model suggests disklike micelles with a negative charge of 13, a disk thickness of 2.6 nm, and a radius of 5.2 nm. This disk thickness is probably unphysically small. The prolate model suggests the micelles have a negative charge of 15, a length of 6.4 nm, and a cross-sectional radius of 1.6 nm. This radius is consistent with the length of 1.7 nm for a fully extended chain of 12 carbon atoms.[24] In any case,

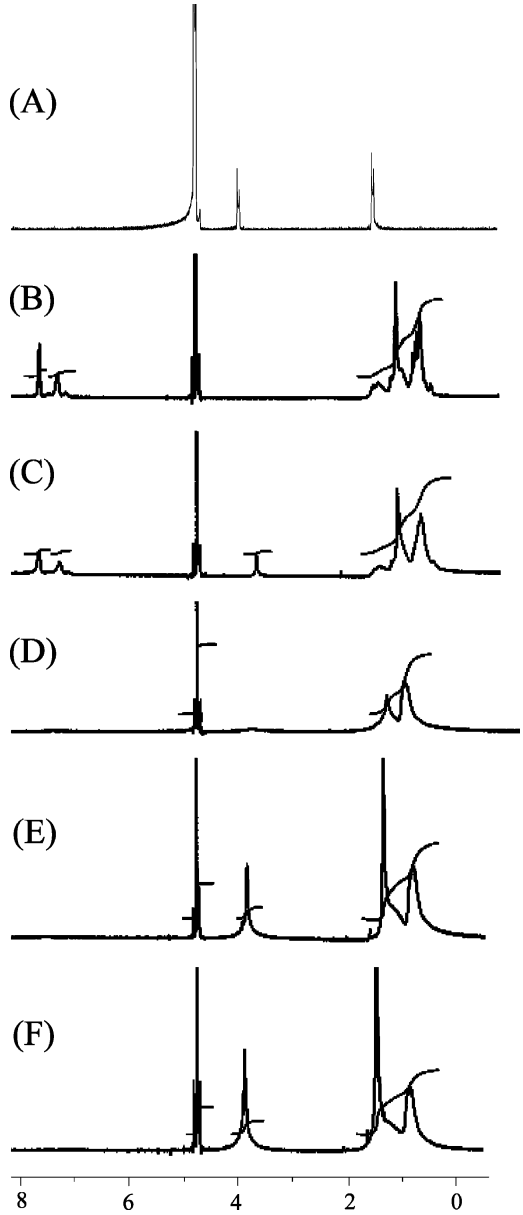


**Figure 10.** NMR spectra of (A) a 5 mM solution of V-44 and solutions of 15 mM SDBS at various V-44 compositions: (B) 0 mM; (C) 2.5 mM; (D) 5 mM; (E) 10 mM; (F) 20 mM. The spectra were obtained 1 day after mixing the stock solutions. Chemical shifts ($\delta$) are in units of ppm.

both models indicate the formation of small and globular micelles with an aggregation number ($N$) of ~100. Scattering from a V-44/SDBS sample made at a similar composition overlaps the scattering data of the RP/SDBS sample except for values of $q < 0.01$ Å$^{-1}$ (Figure 11, open triangles).

**(b) Vesicles: QLS and SANS Results.** Light scattering measurements reveal that larger and more polydisperse vesicles are found in RP/SDBS mixtures than in V-44/SDBS samples having similar concentrations. These vesicles also continue to grow after 6 months of equilibration, and a tiny amount of precipitate is observed. The SANS spectra for RP/SDBS samples with increasing dilution suggest the presence of vesicles in solution (Figure 12). The data can be fit by a polydisperse core−shell model (Table 3), and the vesicles all have similar sizes, polydispersities, and bilayer thicknesses.

(24) Tanford, C. *The Hydrophobic Effect: Formation of Micelles and Biological Membranes*, 2nd ed.; John Wiley & Sons: New York, 1980.

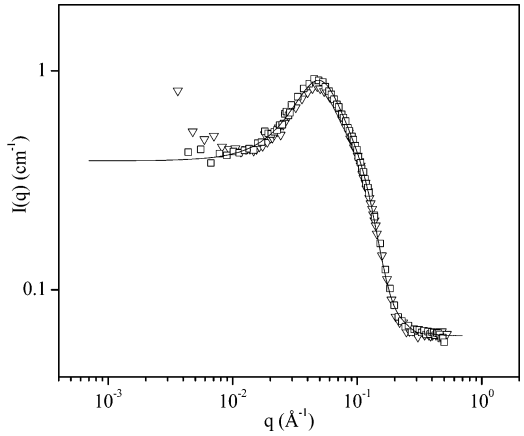


**Figure 11.** SANS spectra for (□) RP/SDBS and (▽) V-44/SDBS micellar samples at a composition of 2.5 mM hydrotrope and 30 mM SDBS. The experimental spectra are essentially identical and were fit assuming ellipsoidal particles for the form factor and the Hayter and Penfold rescaled mean spherical approximation for $S(q)$ (see text).

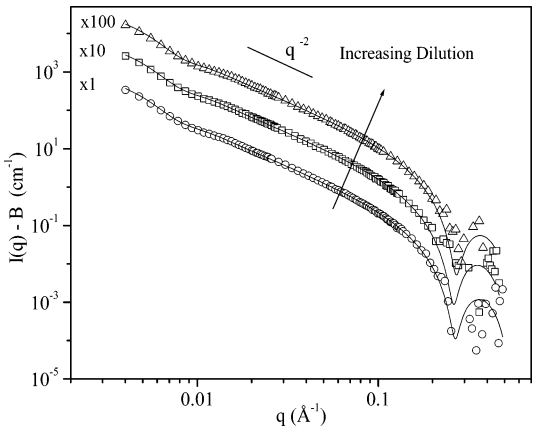


**Figure 12.** SANS spectra for samples within the vesicle region at increasing dilution and a constant RP/SDBS molar ratio of 1:2. The total surfactant concentrations are (○) 32 mM, (□) 24 mM, and (△) 16 mM. The open symbols represent the experimental data and the solid lines the fit to the experimental data using a smeared polydisperse core−shell model. The spectrum at 32 mM is on an absolute scale, and subsequent spectra are shifted upward by factors of 10 and 100 for clarity.

**Table 3. Results from Fitting the Smeared Polydisperse Core−Shell Model to the SANS Spectra from Samples Containing Vesicles at Increasing Dilution and a Constant RP/SDBS Molar Ratio of 1:2 (Figure 12)[a]**

| total concn (mM) | outer diameter (nm) | poly-dispersity | bilayer thickness (nm) | vesicle volume fraction (%) | $\sqrt{\chi^2/N}$ |
|---|---|---|---|---|---|
| 32 | 69 ± 2 | 0.35 ± 0.02 | 2.4 ± 0.1 | 4.7 | 2.6 |
| 24 | 68 ± 1 | 0.34 ± 0.02 | 2.4 ± 0.1 | 3.6 | 2.3 |
| 16 | 66 ± 1 | 0.34 ± 0.02 | 2.3 ± 0.1 | 2.2 | 2.8 |

[a] The quality of the fits is assessed from the reduced $\chi^2$ error between model and data.

Figure 13 and Table 4 show the scattering data, fit results, and parameters for samples having different ratios of RP/SDBS and a constant total molar concentration of 32 mM. Excellent fits are obtained for molar ratios of 1:3.7 RP/SDBS and 1:2.0 RP/SDBS, while $\chi^2$ is larger for 1:1.3 RP/SDBS. The fitted parameters for this sample yield a large polydispersity of 0.6 ± 0.1 and a small vesicle diameter of 32 ± 4 nm. Evidence of the large polydispersity is the absence of the minima at $q \sim 0.01$ Å$^{-1}$.

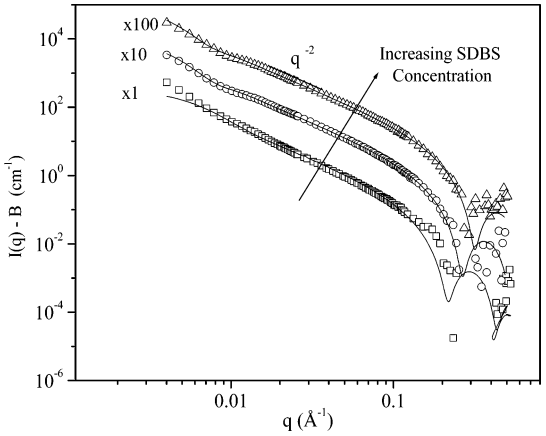


**Figure 13.** SANS spectra for samples at different ratios of RP/SDBS and a total molar concentration of 32 mM. The molar ratios of RP/SDBS are (□) 1:1.3, (○) 1:2.0, and (△) 1:3.7. The open symbols represent the experimental data and the solid lines the fit to the experimental data using a smeared polydisperse core−shell model. The spectrum at a molar ratio of 1:1.3 RP/SDBS is on an absolute scale, and subsequent spectra are shifted upward by factors of 10 and 100 for clarity.

**Table 4. Results from Fitting the Smeared Polydisperse Core−Shell Model to the SANS Spectra from RP/SDBS Samples and with a Total Molar Concentration of 32 mM (Figure 13)[a]**

| RP/SDBS molar ratio | outer diameter (nm) | polydispersity | bilayer thickness (nm) | vesicle volume fraction (%) | $\sqrt{\chi^2/N}$ |
|---|---|---|---|---|---|
| 1:1.3 | 32 ± 4 | 0.6 ± 0.1 | 2.9 ± 0.3 | 2.2 | 7.8 |
| 1:2.0 | 69 ± 2 | 0.35 ± 0.02 | 2.4 ± 0.1 | 4.7 | 2.6 |
| 1:3.7 | 70 ± 2 | 0.37 ± 0.03 | 2.0 ± 0.1 | 6.3 | 3.2 |

[a] The quality of the fits is assessed from the reduced $\chi^2$ error between model and data.

**(c) Cryo-TEM Results.** Vesicles are found in mixtures of RP/SDBS and V-44/SDBS made with a similar concentration of 2.5 mM hydrotrope and 9.8 mM SDBS, although RP/SDBS vesicles are not as spherical as those seen in the V-44/SDBS mixture. RP/SDBS samples also exhibit more elongated vesicles (larger than 100 nm) and bilamellar structures. This is in agreement with the SANS results discussed above that reflect larger sizes for vesicles made with RP and SDBS. The micrographs in Figure 8 are representative of the microstructures seen in each of these phases.

A novel colloidal structure made of multiple closely packed bilayers is also observed by cryo-TEM in equimolar RP/SDBS samples (Figure 14). Figure 14B shows that several vesicle bilayers "fuse" into a thick shell, which, in this case, is more than 10 times thicker than the bilayers usually observed in vesicle walls. The bilayers adhere to one another and apparently fuse, despite the repulsive electrostatic forces that must be present between the bilayers. This unique structure is seen in coexistence with a large number of multilamellar vesicles. Over time, the fused bilayers become thicker, while the population of multilamellar vesicles decreases.

**Vesicle Formation in TMI/SDBS Mixtures.** Upon mixing TMI and SDBS, metastable vesicular aggregates spontaneously form in mixtures with a molar ratio TMI/SDBS > 1. However, over a period of 2 weeks, the blue color characteristic of vesicular dispersions gradually fades until all solutions are transparent. This transition suggests a collapse of the vesicle structures. Upon lowering the pH to 9, the solutions immediately turn bluish again as a result of the spontaneous vesicle formation. The bluish color is preserved even when the pH is decreased to 3. Vesicle formation at 25 °C was studied for three different paths of constant SDBS composition (10, 20, and 40 mM) and increasing TMI·$n$HCl ($n$ = 1 or 2) composition. Vesicles form in solutions with a pH ranging from 10 to 3. The pHs and sizes measured by QLS for representative samples after 6 weeks of equilibration are shown in Tables 5 and 6. Along each of the SDBS paths, the now typical transition from micelles to vesicles to precipitate is observed. In solutions for which $n$ = 2, the molar ratio of TMI/SDBS at which aggregates precipitate is larger than that in mixtures of V-44/SDBS and RP/SDBS. No correlation between pH and vesicle size is observed. At equimolar compositions, vesicles of various sizes similar to those shown in Figure 8B and C were observed by cryo-TEM.

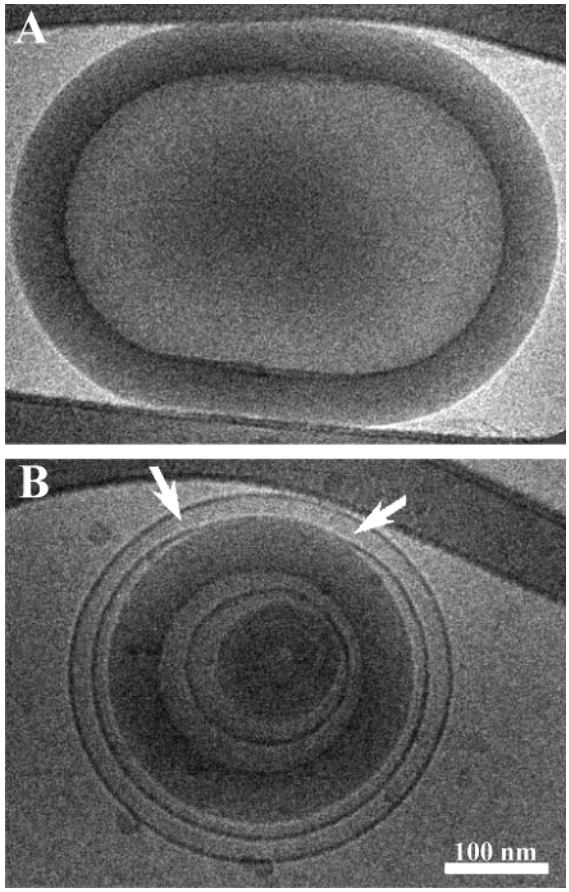


**Figure 14.** Novel bilayer complexes found in a 5 mM equimolar RP/SDBS mixture. The structures are formed by fusion of individual bilayers one onto the other, leading to a thick membrane, as highlighted by the white arrows in part B.

## Discussion

Dilute solutions of SDBS form a wide range of microstructures when combined with compounds containing imidazoline functional groups. V-44, RP, and TMI transform spherical micelles of SDBS to mixed aggregates of lower curvature including small unilamellar vesicles. These transformations are likely the result of attractive interactions between the negatively charged benzenesulfonate headgroups and the positively charged imidazoline groups. Evidence of this is the critical aggregation concentration (cac) of the mixtures, which is an order of magnitude lower than the critical micelle concentration (cmc) of SDBS surfactant. On the other hand, the imidazoline compounds studied in this work do not have a cmc and are best classified as hydrotropes.[25] As such, they are short-chained, water-soluble, weakly surface-

**Table 5. pHs and Average Diameters of Aggregates Formed in Mixtures of SDBS/TMI·HCl after 6 Weeks of Equilibration[a]**

| SDBS/ TMI·HCl (mM) | pH | QLS size (nm) | SDBS/ TMI·HCl (mM) | pH | QLS size (nm) |
|---|---|---|---|---|---|
| 10:5 | 10.1 | 6 | 20:10 | 10.0 | 67 |
| 10:15 | 9.5 | 145 | 20:30 | 9.5 | two phases[c] |
| 10:40 | 9.2 | 600[b] | 40:30 | 10.1 | PPT |
| 40:10 | 9.8 | 5 | 40:50 | 9.9 | two phases[c] |

[a] The size is obtained from QLS measurements and the method of cumulants. [b] The samples are turbid, indicating the onset of precipitate formation at higher TMI concentration. [c] The top phase has a turbid appearance, while the bottom phase is oily and has a yellowish color.

**Table 6. pHs and Average Diameters of Aggregates Formed in Mixtures of SDBS/TMI·2HCl after 6 Weeks of Equilibration[a]**

| SDBS/ TMI·2HCl (mM) | pH | QLS size (nm) | SDBS/ TMI·2HCl (mM) | pH | QLS size (nm) |
|---|---|---|---|---|---|
| 10:2.5 | 4.5 | 107 | 20:25 | 3.4 | 103 |
| 10:30 | 2.8 | 131 | 20:30 | 2.8 | 365[b] |
| 10:40 | 2.7 | PPT | 20:50 | 2.6 | PPT |
| 40:10 | 3.4 | 102 | 40:30 | 3.0 | 85[b] |

[a] The size is obtained from QLS measurements and the method of cumulants. [b] The samples are turbid, indicating the onset of precipitate formation at higher TMI concentration.

active species that only show an increased surface activity at high concentrations. For example, the surface tension value 40 mN/m at 835 mM for solutions of V-44 close to saturation is lower than that of other hydrotropes such as sodium salicylate, sodium *p*-toluenesulfonate, and sodium xylenesulfonate.[25] Hydrotropes are known to reduce the critical aggregation concentration of surfactant solutions. This has been studied in detail[26] for mixtures of CTAB or cetylpyridinium chloride with butyl benzenesulfonate hydrotropes, and the same trend is found here.

Hydrotropes containing imidazoline end groups perturb the state of self-assembly of micellar solutions of SDBS by permitting the formation of aggregates such as vesicles and bilayer structures that have a lower surface charge density than that of the SDBS micelles. The transformations from micelles to vesicles are observed for a molar ratio of [V44]/[SDBS] = 0.15, which is smaller than the molar ratio [V-50]/[DODABr] = 0.2 reported by Hubert et al.[13] to trigger the formation of twinned vesicle−polymer architectures. Our results support and confirm Hubert et al.'s observations and show that molecules introduced as free-radical initiators disrupt the self-assembly of surfactant colloids.

Below a molar ratio of 0.15, V-44 and RP still disrupt SDBS micelles. SDBS forms spherical micelles of 2.5 nm in diameter as measured by QLS, but the micelles elongate in the presence of V-44 or RP. Thus, micelles of ∼4 nm are observed by cryo-TEM (Figure 3A) for samples prepared with a composition of hydrotrope/SDBS that is within the micellar region. This size is consistent with the size measured by QLS of 2−6 nm and with the sizes obtained from SANS analysis. The population of larger spherical structures shown in Figure 3B for aged micellar samples is likely small precipitate particles and may account for the small enhanced scattering observed in the V-44/SDBS scattering data at low $-q$ values.

Unlike vesicles formed in other mixtures of hydrotropes and surfactants,[7] the unilamellar vesicles seen in these imidazoline/SDBS mixtures are small (<110 nm), the mole ratio of hydrotrope to surfactant is small (<0.9), and vesicles form without the need of removing the counterions. They result from simply mixing a micellar solution and a hydrotropic solution at the proper concentrations.

The transition from micelles to vesicles to precipitate can be followed by NMR. NMR spectra show that the interface of vesicle structures in V-44/SDBS mixtures is more rigid than that of wormlike micelles. The broader signals observed for the hydrogen atoms belonging to the imidazoline and benzenesulfonate moieties in the spectrum of the micellar sample disappear upon vesicle formation. This disappearance is usually observed for transitions in which the chemical species precipitate.[22] The absence of these lines under conditions where precipitate does not form implies that most of the V-44 hydrotrope, together with the SDBS, forms part of the vesicle bilayers and that the headgroups in the bilayers are less mobile than the headgroups in wormlike micelles. In the NMR spectra of solutions containing wormlike micelles, the lines are broad and unresolved, as the molecular motion of the ions is restricted.[22,23] The broadening of the lines suggests a binding mechanism consistent with the transition from micelles to vesicles. As the hydrotrope binds to the oppositely charged SDBS molecules, the surface charge density is lowered. This lowers the area per headgroup, which consequently drives up the surfactant packing parameter and favors aggregates of lower curvature.

In addition to favorable electrostatic interactions among the headgroups, two other factors appear to be important for micelles to transform into vesicles. First, the use of branched SDBS hydrophobe with its large volume is crucial for vesicle formation based on the packing parameter criteria.[27] Vesicles do not form at the same range of compositions when V-44 or RP is combined with sodium dodecyl sulfate, a 12-carbon linear chain anionic surfactant, or with sodium octylbenzenesulfonate, an 8-carbon linear chain anionic surfactant. The geometry of SDBS probably also plays a role in the transformation to vesicles rather than uniaxial growth to rodlike objects. The latter transition is typical for mixtures of surfactant and hydrotrope and gives rise to highly viscous solutions even at low hydrotrope concentrations.[28]

Second, the imidazoline groups need to be fully protonated, which necessitates the solution pH to be below the p$K_a$ of the imidazoline moieties. While unstable vesicles form in solutions of SDBS with the basic form of TMI, stable vesicles are obtained only in more acidic solutions of TMI·*n*HCl/SDBS ($n$ = 1 or 2). Stability here implies that the vesicular phase persists even after a period of months. For the solutions with $n = 2$, the transition from vesicles to precipitate occurs at a much higher molar ratio of TMI than that of V-44 or RP. Vesicles are observed even in solutions containing more TMI than SDBS. At $n = 2$, the acidic conditions are similar for all imidazoline compounds, so that both imidazoline end groups are protonated and the chlorine ion concentrations are identical. Given that TMI forms vesicles with SDBS over a larger concentration range than the other hydrotropes suggests that the flexibility and length of the alkyl chain in TMI

(25) Balasubramanian, D.; Srinivas, V.; Gaikar, V. G.; Sharma, M. M. *J. Phys. Chem.* **1989**, *93*, 3865.
(26) (a) Bhat, M.; Gaikar, V. G. *Langmuir* **1999**, *15*, 4740. (b) Bhat, M.; Gaikar, V. G. *Langmuir* **2000**, *16*, 1580.
(27) Israelachvili, J. *Intramolecular & Surface Forces*, 2nd ed.; Academic Press: London, 1991.
(28) (a) Hassan, P. A.; Valaulikar, B. S.; Manohar, C.; Kern, F.; Bourdieu, L.; Candau, S. J. *Langmuir* **1996**, *12*, 4350. (b) Rao, U. R. K.; Manohar, C.; Valaulikar, B. S.; Iyer, R. M. *J. Phys. Chem.* **1987**, *91*, 3286.

plays a role in setting its interactions with SDBS molecules. Increasing the pH causes TMI/SDBS vesicles to disappear, but they form again as the pH drops. The fact that stable vesicles form immediately in TMI/SDBS mixtures by lowering the pH in the absence of shear supports the statement that vesicles form spontaneously. The contribution of electrostatic screening due to the chloride ions and a detailed study of the phase transitions as a function of pH will be reported elsewhere.

The scattering results of vesicle bilayer thickness and polydispersity shown in Tables 1 and 3 for mixtures of V-44/SDBS and RP/SDBS, respectively, are consistent with the parameters obtained for vesicles in mixtures of SDBS and CTAT.[12] These results also confirm QLS measurements indicating that the vesicles formed in RP/SDBS mixtures are somewhat larger and more polydisperse than the vesicles formed in mixtures of V-44 and SDBS. The presence of side products other than RP could perhaps account for these differences in size. The larger $\chi^2$ value, bilayer thickness, and polydispersity obtained for the sample with a molar ratio of 1:1.3 RP/SDBS suggest that the measured scattering could result from the presence of multilamellar vesicles, in agreement with the cryo-TEM results that show numerous vesicles, one embedded inside the other, in samples close to equimolar compositions.

Fused bilayer structures similar to those shown in Figure 14A have been reported by Bergstrand et al.[29] for a dilute aqueous dispersion of egg phosphatidylcholine and more recently by Kawasaki et al.[8] for a sediment consisting of aggregated multilamellar vesicles. Elsewhere, multilamellar vesicles are seen as onionlike structures in which each of the bilayers can be clearly distinguished. Here, cryo-TEM micrographs show unambiguous evidence that vesicle bilayers stack to form a thick shell. The fact that the vesicles are negatively charged and that double-headed positively charged molecule groups are in solution could facilitate the formation of these structures. NMR results show that imidazoline compounds are intercalated among the SDBS molecules forming the vesicles, thus suppressing the electrostatic repulsion between the bilayers. Cryo-TEM micrographs show that at equimolar compositions there are vesicles with multiple embedded layers. Consequently, several of these layers are in close proximity, so it is possible that with time an imidazoline molecule could have an end group inserted in one vesicle bilayer and the other imidazoline end might insert into the bilayer of a concentric vesicle. We speculate that once an imidazoline molecule electrostatically bridges two different bilayers, the resulting fused bilayer is quite stable.

The mechanism of stabilization of the unilamellar vesicles can be determined by fitting the vesicle size distributions (Figure 9) to theoretical expressions that allow determination of the effective bilayer bending constant ($K$) and the radius of the vesicle with minimum curvature energy ($R_0$).[30] When $K \gg k_BT$, the most probable state is vesicles of a preferred size which are stabilized by a particular spontaneous curvature. Other radii are disfavored energetically; hence, the vesicles have a narrow size distribution.[30,31] When $K \sim k_BT$, entropic effects ensure stability of the vesicular phase in the dilute limit. In this limit, vesicles are stabilized by Helfrich undulation repulsions.[32] Since the spontaneous curvature does not pick out a particular vesicle radius, such vesicles have a much broader size distribution than those stabilized by the spontaneous curvature.

As described by Jung et al. and Coldren et al.,[21,30] $K$ and $R_0$ can be obtained from

$$C_N = \left\{ C_M \exp\left[ \frac{-8\pi K}{k_B T} \left( 1 - \frac{R_0}{R} \right)^2 \right] \right\}^{R^2/R_0^2} \qquad (8)$$

under the following assumptions: (i) the vesicles are spherical, (ii) their bilayer thicknesses and the Debye lengths of the ionic species are small compared to the radii of curvature, (iii) ideal mixing of the vesicles, and (iv) dilute vesicle dispersions. In eq 8, $C_N$ and $C_M$ are the number fractions of vesicles of sizes $M$ and $N$, respectively, where $M = 8\pi R_0^2/A_0$ and $N = 8\pi R^2/A_0$ ($A_0$ is the mean molecular area).

These conditions are applicable here. A best fit to eq 8 yields $K = (0.35 \pm 0.02)k_BT$ and $R_0 = 30.0 \pm 0.4$ nm for the 1 month old sample. Likewise, $K = (0.16 \pm 0.01)k_BT$ and $R_0 = 46 \pm 3$ nm for the 6 month old sample. Since the bending constant ($K$) is of the order of $k_BT$ in both cases, the vesicles are stabilized by fluctuations. The same stabilization mechanism has been found for unilamellar vesicles in CTAB/perfluorooctanoate acid, CTAB/sodium octyl sulfate, and CTAT/SDBS solutions.[21,30]

Broadening of the distribution and the increase in $R_0$ with time suggest the vesicles have not reached their final equilibrium size after aging for 6 months. This is also confirmed by QLS measurements (Figure 4) for vesicle samples at other compositions. Analogous observations have been previously reported for other catanionic vesicles, in which the equilibration times can be long, for example, from weeks to months.[4,33] During this period, polydispersity and vesicle size continuously increase, as observed here for the hydrotrope/SDBS vesicles.

## Conclusions

In summary, we present here novel examples of colloidal assemblies formed by an anionic surfactant and compounds bearing imidazoline moieties. At high concentrations, V-44 initiator is a weak surface-active agent and acts as a hydrotrope in SDBS micellar solutions. At 25 °C, V-44 decomposes slowly, mainly into RP, and the equilibrium phase diagrams of V-44/SDBS and RP/SDBS are similar. Both systems exhibit regions of micelles, vesicles, precipitate and bilayers, and vesicles coexisting with precipitate. A V-44 analogue lacking the azo group and with a linear middle chain also forms stable unilamellar vesicles over a wide range of compositions when the solution pH is lower than the p$K_a$ of the imidazoline moiety.

**Acknowledgment.** We acknowledge the support of the National Science Foundation CTS-9814399 and a NSF graduate fellowship to Y.I.G. The National Institute of Standards and Technology, U.S. Department of Commerce, provided the neutron scattering facilities used in this work, which were supported in part by the NSF under Agreement No. DMR-9986442. The cryo-TEM work was performed at the "Cryo-TEM Hannah and George Krumholz Laboratory for Advanced Microscopy" at the Technion Institute of Technology, part of the "Technion Project on Complex Fluids". We are grateful to Federico Cruz for his assistance in making $^{13}C$ NMR measurements and Shiyong Liu for his helpful comments.

LA0493464

(29) Bergstrand, N.; Edwards, K. *Langmuir* **2001**, *17*, 3245.
(30) Jung, H. T.; Coldren, B.; Zasadzinski, J. A.; Iampietro, D. J.; Kaler, E. W. *Proc. Natl. Acad. Sci. U.S.A.* **2001**, *98*, 1353.
(31) Safran, S. A.; Pincus, P.; Andelman, D. *Science* **1990**, *248*, 354.
(32) Helfrich, W. *Z. Naturforsch., A: Phys. Sci.* **1978**, *33*, 305.
(33) Marques, E. F. *Langmuir* **2000**, *16*, 4798.